This article has been accepted for publication in a future issue of this journal, but has not been fully edited. Content may change prior to final publication. Citation information: DOI 10.1109/TTE.2020.3010337, IEEE Transactions on Transportation Electrification

Improving the DC-link Utilization of Nine Switch Boost Inverter suitable for Six Phase Induction Motor

Pinjala Mohana Kishore, Ravikumar Bhimasingu *Member, IEEE*

***Abstract*—Nowadays multi-phase induction drives are used in electric vehicle applications to improve reliability and efficiency. These induction motors are controlled by using a multi-phase voltage source inverter (VSI). As the number of phases increases, the number of switching devices used in multi-phase VSI also increases, which results in a reduction of the system efficiency and increase in the cost. Among these multi-phase drives, the six-phase drive is used more frequently in electric vehicular industries. For a conventional six-phase VSI requires twelve switches to drive the six-phase machine. Also, conventional six-phase, VSI requires more dc-link voltage than the boost six-phase VSI to drive the six-phase machine. In order to overcome the problems associated with the conventional six-phase VSI controlled six-phase induction drives, this paper proposes a nine-switch boost inverter (NSBI) for six-phase induction drive applications. The proposed NSBI has a single input dc voltage source and it provides six-phase ac output voltages. These six-phase output voltages are regulated by using modified non-sinusoidal pulse width modulation (MNSPWM) technique. The proposed NSBI with a six-phase induction motor is simulated using a MATLAB/Simulink ® and validated using FPGA controlled hardware prototype. The verification of the proposed system during load torque variations, winding failure conditions are carried out.**

***Index Terms*—Multi-port converters; Six-phase induction drive; dc-link utilization; Boost inverters; Single stage converters; Optimal PWM; Nine switch inverter.**

I. Introduction

Multi-phase induction motors are promising concepts in many industrial applications where fault-tolerant capability is a crucial design feature such as electric vehicles, aerospace, shipboard systems, and electric traction applications [1]. The number of phases are increase in induction motor, it provides good sinusoidal distribution, which reduces the harmonic current and torque ripples compare to three-phase machine [2]. A multi-phase motor is better than the 3-phase motor for fault-tolerant condition. One-phase or dual-phase open circuit faults occur, the motor can remains operate using other healthy phases without any additional hardware and control [3], [4]. The winding arrangements under one-phase and dual-phase open fault conditions are presented in [5]. The fault-tolerant control algorithms of multi-phase induction machines are reported in [6]–[8] for the open-phase faults. Multi-phase induction drives offers many outstanding merits than the conventional three-phase drives, which includes [9];

- Lesser per phase voltage or current and dc-link current harmonics,
- Improving torque density by harmonic injection,
- Improving flux distribution with less torque ripple,
- Improving drive efficiency because of lower space harmonic current in the stator field,
- The voltage and current rating per inverter leg is reduce,
- Greater fault tolerant than three-phase motors, because the degrees of freedom increase with number of phases.

Out of the multi-phase drives, six phase motors have met a special interest in the literature available [10]. The six-phase windings are divided into two three-phase winding sets, which has two possible winding configurations based on the wining arrangement between the two three-phase winding sets; (i) symmetrical machine: dual three-phase windings with 60^o shift between them (ii) asymmetrical machine: dual three-phase windings with 30^o shift between them. These six-phase machines are controlled by using different inverter topologies, such as traditional two level inverter [10], multi-level inverter [11] and modular multi-level inverter [12]–[15]. As well as, the two stage converter, Z-source inverters [16]–[23], switched capacitor converters [24], split source inverter (SSI) [25]–[30] are also used to drive the induction motor. Among these converters, SSI [25] has meritorious performance in terms of switching voltage stress, less device count, and continuous input current.

The nine switch inverter (NSI) [31], [32] is a presented in the literature to supply the two 3-phase outputs(i,e., six-phase output voltages) with a lesser device count compared with traditional two-level inverter (Fig. 1a). The NSI having advantages of lesser device count, lesser driver cost, and increased reliability. And the dual three phase loads of NSI are independently control [33], [34].

The main disadvantage of NSI is its lesser utilization of dc-link voltage than the conventional VSI. NSI requires a more input voltage than conventional VSI for achieving the desired outputs. When using a NSI with asymmetrical winding machine and symmetrical winding machines, the output voltage requirements are 20% and 33.33% lesser than nominal voltages [35]–[39]. The required dc link voltage in NSI can

This work is supported by Project No: EMR/2016/003957, sponsored by Science and Engineering Research Board (SERB), a statutory body under the Department of Science and Technology (DST), Government of India.

Authors are with the Department of Electrical Engineering, Indian Institute of Technology, Hyderabad (IIT Hyderabad), India, e-mail: ee14resch01006@iith.ac.in, ravikumar@ee.iith.ac.in.

This article has been accepted for publication in a future issue of this journal, but has not been fully edited. Content may change prior to final publication. Citation information: DOI 10.1109/TTE.2020.3010337, IEEE Transactions on Transportation Electrification

be increased by boosting the input voltage. In [40]–[43], two stage conversions based on NSI with boost converter and NSI with ZSI are proposed for EV applications. Because of the two stage conversions, the overall system performance reduces and the size, weight, cost, and complexity increases. In [44] dual input NSI was introduced for renewable energy applications.

Considering these limitations, this paper proposes a six-phase Nine Switch Boost Inverter (NSBI), which uses lesser input dc voltage as compared to the conventional six-phase VSI to drive a given six-phase induction motor. The six phase voltages applied to the motor are regulated by using the developed Modified Non-Sinusoidal Pulse-Width- Modulation (MNSPWM) technique adopted from [37]. The main features of the proposed NSBI is as follows:

- Provides six phase boost ac outputs in a single-stage conversion;
- Continuous input currents and dc-link voltage;
- Higher ac and dc voltage gains;
- Can be used for variable frequency operations;
- Can be operated during winding failure conditions as a reduced phase operating induction machine;
- Improves the input dc-link voltage utilization;

The main contributions of this paper are

1. Proposed the NSBI topology for improving the dc-link utilization of six-phase induction drive (discussed in Section-II).
2. Adopted the discontinues modulation scheme from [37] and modified it suitable for the operation of the proposed NSBI converter to drive the six-phase motor in symmetrical or asymmetrical winding configuration (discussed in Section-II.C).
3. Derived the optimal modulation region of NSBI (discussed in Section-II.C.4).
4. Mathematical, and simulation analysis of the NSBI fed six phase induction drive under normal, and winding failure conditions (discussed in Section-III, Section-IV).
5. Hardware development and experimental verification of the proposed NSBI fed six phase induction drive during normal and faulty conditions (discussed in Section-IV).

The paper is organized as follows: Section II discus the description, operation, and modulation schemes of NSBI. Simulation and hardware results of the NSBI are discussed in Section III. And, section IV provide conclusions based on the results.

II. Nine Switch Boost Inverter (NSBI)

A. Description of NSBI

The NSBI topology is shown in Fig. 1b along with its connections to six phase induction motor (called as NSBI drive). The proposed NSBI has "three parallel legs (leg A, leg B, leg C), and each leg consists of three switches connected in series. This structure is an extended version of two-level VSI. The input dc voltage source (V_{dci}) is connected to the upper inverter switches of leg A, Leg B and leg C through inductor (L) and diodes (D_1, D_2 and D_3) in series at A, B and C points. The capacitor C is connected in parallel to these

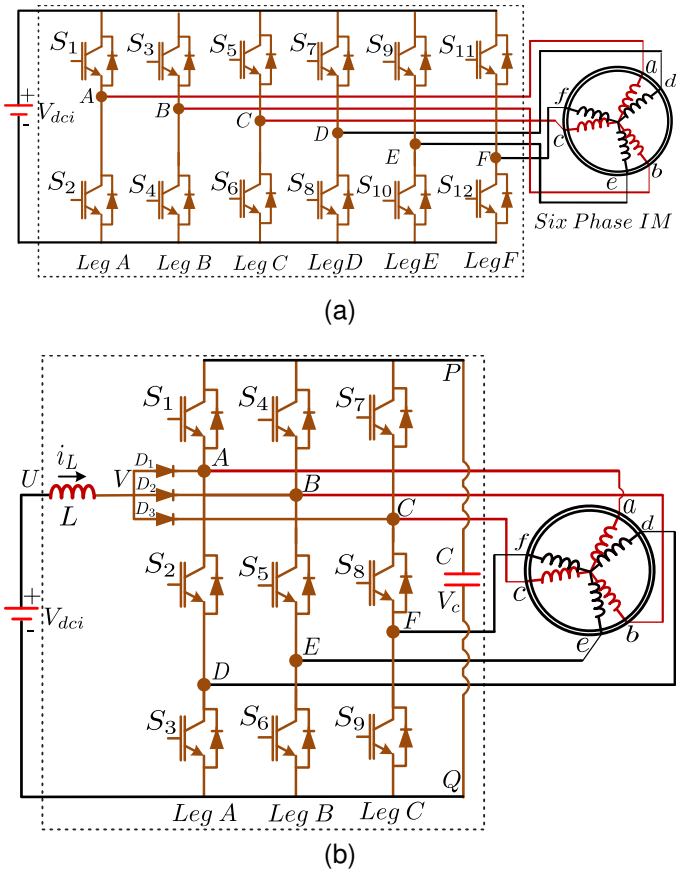

Fig. 1. The six-phase induction motor is controlled by using a) Conventional six-phase voltage source inverter b) Proposed nine switch boost inverter (NSBI).

legs (at points P and Q)". The voltage across the capacitor is V_c. The outputs of the lower and upper inverter of the NSBI are connected to six-phase induction machine. One set of three phase windings are connected to upper inverter at A, B and C terminals and another set of three phase windings are connected to lower inverter at D, E and F terminals. The spatial displacement between these two phases winding sets can be either 30^o or 60^o depending on the asymmetrical or symmetrical winding configuration. The six-phase induction machine is modeled as per the details given in [45].

B. Operation of NSBI

Regarding NSBI switching operation, the gating signals of leg A are generated by comparing the reference signals d_A and d_D (upper and lower reference signals per phase) with a carrier signal v_C , as shown in Fig. 2a. If the reference signal of upper inverter d_A is more than the v_C, then the upper switch S_1 will be turned ON, otherwise, it will be turned OFF. In the same way, if the reference signal of lower inverter d_D is lesser than the v_C, then lower switch S_3 will be turned ON, otherwise, it will be turned OFF. Thereafter, both the gate signals of upper and lower switches (S_1 and S_3) are given to the XOR logical operation in order to generate the gate signal for S_2. The implementation of the gating signal generation is shown in Fig 2b.

This article has been accepted for publication in a future issue of this journal, but has not been fully edited. Content may change prior to final publication. Citation information: DOI 10.1109/TTE.2020.3010337, IEEE Transactions on Transportation Electrification

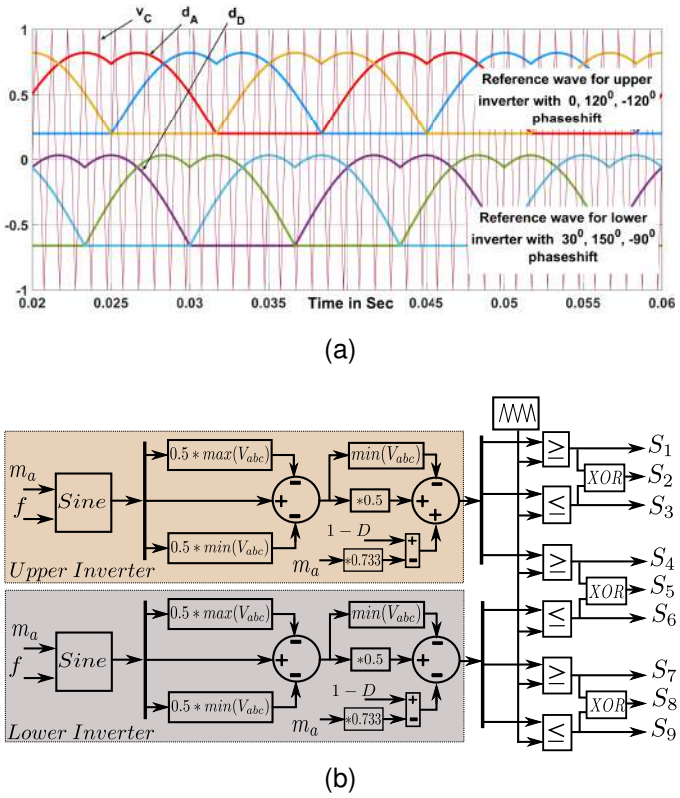

Fig. 2. a) The six phase reference waveforms of MNSPWM, b) Implementation of MNSPWM.

TABLE I
SWITCHING STATES OF NSBI

State	Fig	Switches			Pole Voltages		Cap	L
		S_1	S_2	S_3	V_{AQ}	V_{DQ}		
[N]	3(a)	0	1	1	0	0	D	C
[Z]	3(b)	1	0	1	V_c	0	C	D
[P]	3(c)	1	1	0	V_c	V_c	C	D

C = Charging , D= Discharge

The switching states per phase (leg A) are divided into "State [N], State [Z], State [P]" as shown in Fig. 3, and summarized in Table I. Similar way, the switching states of leg-B and leg-C are in same as that of leg-A. The operation of the NSBI in each switching state is given as follows:

a) State [N] [Fig 3a]: In this state, switches S_2, S_3 are in ON state and switch S_1 is OFF state. Inductor (L) is charged with a duty-ratio of d through switches S_2, S_3 and V_{dci}. The current through inductor L is i_L. The capacitor is discharged to load with a voltage of V_c. Both the upper and lower inverter pole voltages (V_{AQ} and V_{DQ}) are zero.

b) State [Z] [Fig 3b]: In this state, switches S_1, S_3 are ON state and switch S_2 is OFF state. The inductor L discharged its energy through switch S_1, capacitor C and V_{dci}. During this state, capacitor charges to ($V_{dci} + v_L$). Here, V_L is the voltage across inductor L. The upper and lower inverter pole voltages (V_{AQ} and V_{DQ}) are V_c and zero respectively.

c) State [P] [Fig 3c]: In this state, switches S_1, S_2 are ON state and switch S_3 is OFF state. The inductor L discharged its energy through switch S_1, capacitor C and V_{dci}. During this state capacitor charged to $V_{dci}+v_L$. Both the upper and lower inverter pole voltages (V_{AQ} and V_{DQ}) are V_c.

The operation of NSBI is characterized by 27 modes (all three legs) as shown in Fig. 4. The pole voltage (V_{AQ}) is composed by 0 and V_c with respect to negative of dc bus. The line voltage ($V_{AB} = V_{AQ} - V_{BQ}$) is composed by $-V_c$, 0, V_c. The generation of gate signals and line voltages of six phases are shown in Fig. 5. From this, the upper and lower inverter reference signals (d_A, d_B, d_C, d_D, d_E, d_F) are compared with carrier signal v_C and the switching signals are generated. The six-phase voltages are generated based on these switching signals (Fig. 2a), switching states (Table. I) and modes of operation (Fig. 3).

C. Modulation of NSBI

In the process of selecting the suitable modulation technique to NSBI, the sinusoidal PWM (SPWM), third-harmonic PWM (THPWM), and space-vector PWM (SVPWM) schemes are analyzed. Based on the observations while comparing all conventional modulation schemes, this section develops a modified non sinusoidal PWM (MNSPWM) adapted from [37] suitable for the operation of NSBI. After that, the optimal modulation is derived to eliminate the crossover between the upper and lower inverter switches. Following sections describes the operation of various modulation techniques used to compare along with the developed MNSPWM scheme.

1) Sinusoidal PWM Scheme: The SPWM scheme for the NSI driven six-phase machine was given in [31], [32]. The six-phase reference signals for upper and lower inverters are given by

$$v_A = m_a \times sin(\omega t) \tag{1}$$

$$v_B = m_a \times sin(\omega t + \frac{2\pi}{3}) \tag{2}$$

$$v_C = m_a \times sin(\omega t - \frac{2\pi}{3}) \tag{3}$$

$$v_D = m_a \times sin(\omega t + \frac{\pi}{6} + \phi) \tag{4}$$

$$v_E = m_a \times sin(\omega t + \frac{5\pi}{6} + \phi) \tag{5}$$

$$v_F = m_a \times sin(\omega t - \frac{\pi}{2} + \phi) \tag{6}$$

where, $\omega = 2\pi f$, f is fundamental frequency, m_a is modulation index within the linear range of 0 to 1, and ϕ is the phase-shift angle (for symmetrical winding: ϕ is $\pi/6$ and for asymmetrical winding: ϕ is 0).

Based on (1) - (6), in order to arranging the upper and lower signals in the linear modulation range, the dc component offsets $v_{Uoffset} = (1 - m_a)$ and $v_{Loffset} = (m_a - 1)$ are injected. Then, the six-phase duty signals of upper and lower inverters are represents by $d_A^{'}$, $d_B^{'}$, $d_C^{'}$ and $d_D^{'}$, $d_E^{'}$, $d_F^{'}$ respectively as follows:

$$d_A^{'} = v_A + (1 - m_a) \tag{7}$$

$$d_B^{'} = v_B + (1 - m_a) \tag{8}$$

$$d_C^{'} = v_C + (1 - m_a) \tag{9}$$

This article has been accepted for publication in a future issue of this journal, but has not been fully edited. Content may change prior to final publication. Citation information: DOI 10.1109/TTE.2020.3010337, IEEE Transactions on Transportation Electrification

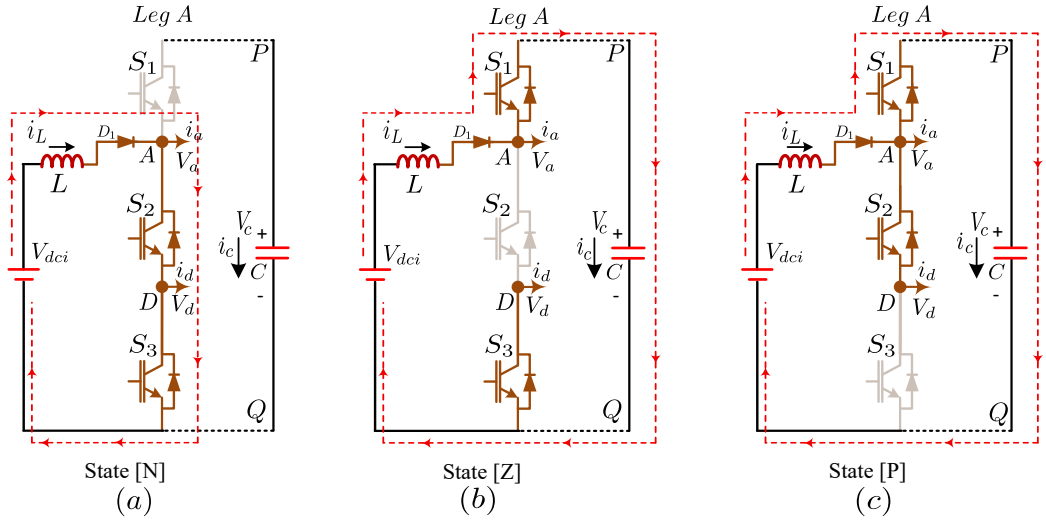

Fig. 3. Operation of the NSBI per phase(leg-A), (a) State [N], (b) State [Z], (c) State [P].

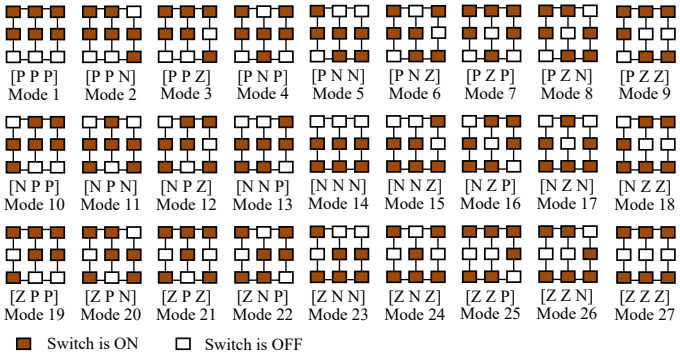

Fig. 4. 27-switching Modes of NSBI.

$$d_D^{'} = v_D + (m_a - 1) \tag{10}$$

$$d_E^{'} = v_E + (m_a - 1) \tag{11}$$

$$d_F^{'} = v_F + (m_a - 1) \tag{12}$$

While using (7) -(12), the output voltage of upper and lower inverters are not disturbed. But, the peak maximum values of output fundamental voltage would be only $0.866 \times m_a \times V_C$.

2) Third harmonic injection PWM: The THPWM technique was used to achieve the higher fundamental output voltages. This technique removes the third harmonic quantities from the fundamental quantity by injecting the third order reference waves. And also, for arranging the upper and lower inverter signals in the linear modulation range, the dc component offsets $v_{Uoffset} = (1 - m_a)$ and $v_{Loffset} = (m_a - 1)$ are injected. With the injections the updated six-phase duty signals of upper and lower inverters are $d_A^{''}$, $d_B^{''}$, $d_C^{''}$ and $d_D^{''}$, $d_E^{''}$, $d_F^{''}$ respectively, which can be expressed in (13)-(18)

$$d_A^{''} = m_a \times sin(\omega t) + \frac{m_a}{6} \times sin(3\omega t) + (1 - m_a) \tag{13}$$

$$d_B^{''} = m_a \times sin(\omega t + \frac{2\pi}{3}) + \frac{m_a}{6} \times sin(3\omega t) + (1 - m_a) \tag{14}$$

$$d_C^{''} = m_a \times sin(\omega t - \frac{2\pi}{3}) + \frac{m_a}{6} \times sin(3\omega t) + (1 - m_a) \tag{15}$$

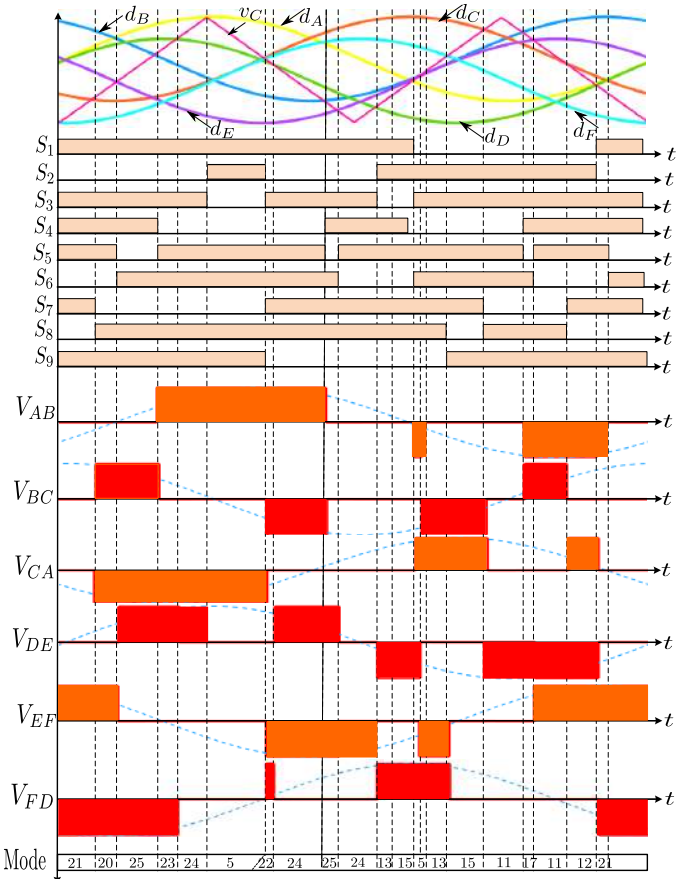

Fig. 5. Generations of gating signals and six-phase voltages of NSBI during different modes of operation.

$$d_D^{''} = m_a \times sin(\omega t + \frac{\pi}{6} + \phi) + \frac{m_a}{6} \times sin(3\omega t) + (m_a - 1) \tag{16}$$

$$d_E^{''} = m_a \times sin(\omega t + \frac{5\pi}{6} + \phi) + \frac{m_a}{6} \times sin(3\omega t) + (m_a - 1) \tag{17}$$

$$d_F^{''} = m_a \times sin(\omega t - \frac{\pi}{2} + \phi) + \frac{m_a}{6} \times sin(3\omega t) + (m_a - 1) \tag{18}$$

3) Space vector PWM: The SVPWM technique was used to achieve the higher fundamental output voltages. To increase the linear modulation range of sinusoidal reference signal, zero-sequence signals (ac component(v_{U0}, v_{L0})) are injected. Due to the added ac component, the modulation index of reference wave becomes lesser peak magnitude than the carrier signal peak, the modulation index can be increased from 1 to 1.15 such that desirable signal peak magnitude is equal to the carriers peak.

The injected zero sequence ac components v_{U0} and v_{L0} are expressed as

$$v_{U0} = -\frac{1}{2}[max(v_A, v_B, v_C) + min(v_A, v_B, v_C)] \quad (19)$$

$$v_{L0} = -\frac{1}{2}[max(v_D, v_E, v_F) + min(v_D, v_E, v_F)] \quad (20)$$

Similar to the SPWM, the necessary dc component offsets $V_{Uoffset} = (1 - m_a\frac{\sqrt{3}}{2})$ and $V_{Loffset} = (m_a\frac{\sqrt{3}}{2} - 1)$ are injected into corresponding (1)-(6). Then, the six-phase duty signals of upper and lower inverters are d_A^*, d_B^*, d_C^* and d_D^*, d_E^*, d_F^* respectively, which can be expressed as follows:

$$d_A^* = v_A + v_{U0} + v_{Uoffset}^* \quad (21)$$

$$d_B^* = v_B + v_{U0} + v_{Uoffset}^* \quad (22)$$

$$d_C^* = v_C + v_{U0} + v_{Uoffset}^* \quad (23)$$

$$d_D^* = v_D + v_{L0} + v_{Loffset}^* \quad (24)$$

$$d_E^* = v_E + v_{L0} + v_{Loffset}^* \quad (25)$$

$$d_F^* = v_F + v_{L0} + v_{Loffset}^* \quad (26)$$

Based on (21) - (26), the achieved fundamental output voltages of upper inverter and lower inverter are 15.5% higher than the SPWM scheme without any impacts on the ac and dc output waveforms. So, proposed NSBI have maximum input dc-link voltage utilization for the m_a of 1.15.

4) Modified Non-Sinusoidal PWM (MNSPWM): Using SPWM, SVPWM, and THPWM schemes, the six-phase stator currents, inductor currents and capacitor voltages of NSBI in asymmetrical and symmetrical winding configurations are plotted in Fig. 6a and Fig. 6b respectively. It is observed that, the inductor ripple current and capacitor ripple voltage are more due to low frequency component that are present in the SPWM, SVPWM, THPWM schemes. In order to remove the lower frequency component present in the inductor ripple current and capacitor ripple voltage, in this paper the MNSPWM is developed based on the concept of the PWM scheme presented in [37] by increasing the discharging time of inductor current and capacitor voltage. This is achieved by decreasing the duration of state [Z] with out disturbing the other states.

The six-phase reference signals of MNSPWM scheme are generated by removing $min(v_A, v_B, v_C)$ from upper inverter duty signals (21)-(23) and $min(v_D, v_E, v_F)$ from lower inverter duty signals (24)-(26) respectively. These are expressed as follows:

$$d_A = \frac{1}{2}(v_A + v_{U0}) - min(v_A, v_B, v_C + v_{U0}) + v_{Uoffset}^* \quad (27)$$

$$d_B = \frac{1}{2}(v_B + v_{U0}) - min(v_A, v_B, v_C + v_{U0}) + v_{Uoffset}^* \quad (28)$$

$$d_C = \frac{1}{2}(v_C + v_{U0}) - min(v_A, v_B, v_C + v_{U0}) + v_{Uoffset}^* \quad (29)$$

$$d_D = \frac{1}{2}(v_D + v_{L0}) - min(v_D, v_E, v_F + v_{l0}) + v_{Loffset}^* \quad (30)$$

$$d_E = \frac{1}{2}(v_E + v_{L0}) - min(v_D, v_E, v_F + v_{l0}) + v_{Loffset}^* \quad (31)$$

$$d_F = \frac{1}{2}(v_F + v_{L0}) - min(v_D, v_E, v_F + v_{l0}) + v_{Loffset}^* \quad (32)$$

The equations (27)-(32) are used to generate the six-phase voltages of NSBI. And the dc gain ($\frac{V_c}{V_{dci}}$) and ac gain ($\frac{V_{AN}}{V_{dci}}$) of NSBI can be calculated by, [27], [46],

$$\frac{V_{AN}}{V_{dci}} = \frac{(2\pi - 1) \times m_a}{(2\sqrt{3}\pi) - (\pi + 2) \times (\sqrt{3}m_a)} \quad (33)$$

$$\frac{V_c}{V_{dci}} = \frac{2\pi}{(2\pi) - (\pi + 2) \times m_a}. \quad (34)$$

Finally, the inductor and capacitor values of NSBI are calculated by,

$$L = \frac{m_a \times V_{dci}}{f_s \times (\Delta I_L)} \quad (35)$$

$$C = \frac{(1 - m_a) \times I_L}{f_s \times (\Delta V_c)}. \quad (36)$$

where Δi_L and ΔV_c are the change in inductor current ripple and dc-link voltage ripple respectively, f_s is the switching frequency.

5) Optimal Modulation: The upper and lower inverter reference signals of NSBI should be arranged in the linear modulation range without crossover. So, the PWM technique for NSBI requires optimal values of modulation index to overcome the crossover between the upper and lower reference signals (d_A and d_D) as shown in Fig. 7. The upper inverter reference signal should be higher than the lower inverter reference signal to avoid the crossover for the entire period [37].

So, consider phase A, the upper inverter reference signal (d_A) and the lower inverter reference signal (d_D) are related as,

$$d_A \geq d_D \quad (37)$$

Substituting (d_A) and (d_D) in the (37), the following inequality equation is obtained,

$$\left(m_a \times \sin(\omega t + \theta) + (1 - \frac{\sqrt{3}m_a}{2})\right) \geq \left(m_a \times \sin\omega t + (\frac{\sqrt{3}m_a}{2} - 1)\right. \quad (38)$$

the (38) can be further simplified as

$$m_a \leq \left(\frac{2}{2 - 2[sin(\frac{\theta}{2}) \times \cos(\frac{2\omega t + \theta}{2})]}\right) \quad (39)$$

The ωt changed from $(-\pi$ to $\pi)$, the cosine term will varied between -1 (when ωt = $(-\pi - \frac{\theta}{2})$ and $(\pi - \frac{\theta}{2})$) and 1 (when ωt = $-\frac{\theta}{2}$). So, it can be further simplified as

$$m_a \leq \left(\frac{1}{1 + sin(\frac{\theta}{2})}\right) \quad for\ 0 \leq \theta \leq \pi \quad (40)$$

This article has been accepted for publication in a future issue of this journal, but has not been fully edited. Content may change prior to final publication. Citation information: DOI 10.1109/TTE.2020.3010337, IEEE Transactions on Transportation Electrification

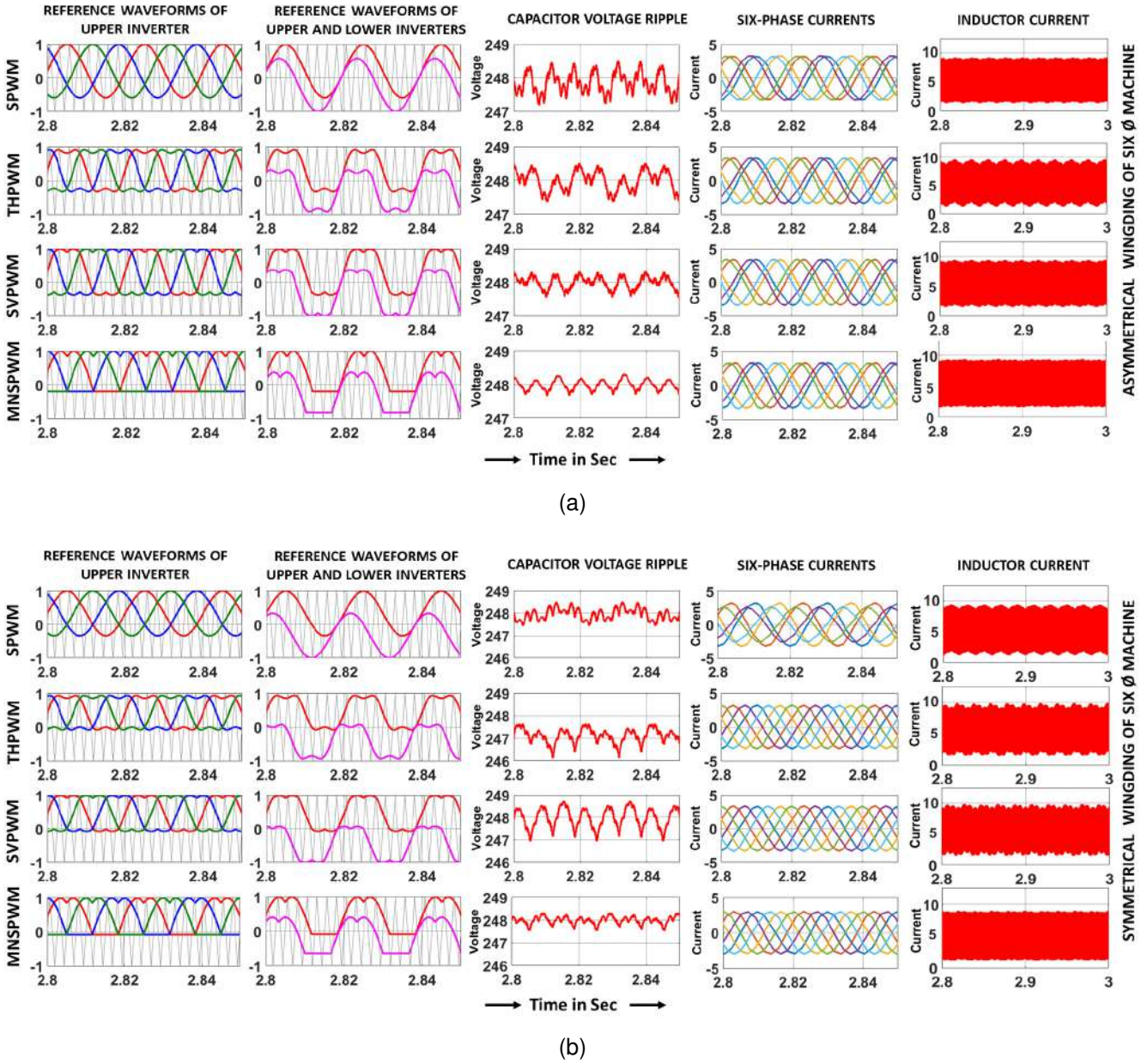

Fig. 6. The comparison of SPWM, THPWM, SVPWM, MNSPWM of a) Asymmetrical winding six phase machine, b) Symmetrical winding six phase machine.

For the symmetrical winding configuration the θ should be $\pi/3$ and the optimal modulation index is 0.677. Similarly, for the asymmetrical winding configuration the θ should be $\pi/6$ and the optimal modulation index is 0.794.
Similarly, the optimal m_a can be derived based on (40) for the other PWM schemes, and are tabulated in Table. III.

6) Comparison of PWM Schemes applied to NSBI: The comparison of PWM, SVPWM, THPWM and MNSPWM schemes applied to symmetrical and asymmetrical winding configurations are plotted in Fig. 6. For comparison purpose, the parameters of NSBI are considered as $V_{dci} = 100V$, $I_{Lmax} = 10A$, $f_s = 5kHz$, $f = 50Hz$ to achieve outputs of $V_{AQ} = 125V$, $I_a = 3A$.

From the Fig 6 and Table III, it is observed that the

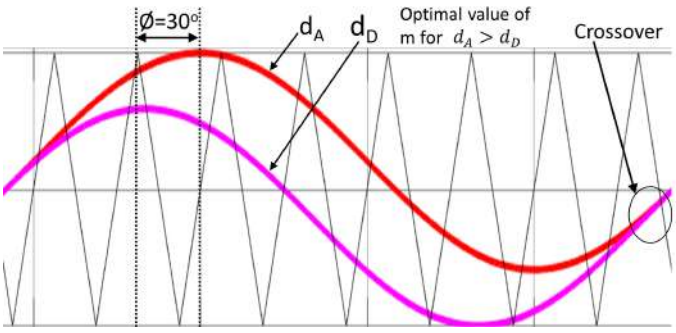

Fig. 7. Optimal modulationindex of upper and lower inverter reference waveforms.

This article has been accepted for publication in a future issue of this journal, but has not been fully edited. Content may change prior to final publication. Citation information: DOI 10.1109/TTE.2020.3010337, IEEE Transactions on Transportation Electrification

TABLE II
THE DUTY-RATIO, AC AND DC GAIN OF MODULATION SCHEMES

	d	$\frac{V_c}{V_{dci}}$	$\frac{V_{AN}}{V_{dci}}$
SPWM	$\frac{1}{\sqrt{2}} + \frac{3\sqrt{3}}{4\pi} m_a$	$\frac{4\pi}{\sqrt{2}\pi - 3\sqrt{3} m_a}$	$\frac{2\pi m_a}{\sqrt{2}\pi - 3\sqrt{3} m_a}$
THPWM	$\frac{1}{2} + \frac{3}{2\pi} m_a$	$\frac{2\pi}{\pi - 3 m_a}$	$\frac{2\pi m_a}{\pi\sqrt{3} - 3\sqrt{3} m_a}$
SVPWM	$(\frac{1}{2} + \frac{3}{2\pi}) m_a$	$\frac{2\pi}{2\pi - (\pi+3) m_a}$	$\frac{2\pi m_a}{2\sqrt{3}\pi - (\pi+3)\sqrt{3} m_a}$
MNSPWM	m_a	$\frac{2\pi}{2\pi - (\pi+2) m_a}$	$\frac{(2\pi-1) m_a}{2\sqrt{3}\pi - (\pi+2)\sqrt{3} m_a}$

TABLE III
COMPARISON OF PWM SCHEMES APPLIED TO NSBI

	m_a	d	$L(mH)$	$C(\mu F)$	$V_c(Volts)$
SPWM	0.59	0.723	4.1	860	320
THPWM	0.62	0.86	3.6	620	380
SVPWM	0.64	0.65	3.2	440	390
MNSPWM	0.79	0.79	2.8	320	410

modulationindex of asymmetrical winding configuration is higher than the symmetrical winding configuration, because of the derived optimal modulation index value is higher for asymmetrical winding configuration. While using the SPWM scheme, the six phase stator currents are disturbed and also the modulation index value is limited to 0.589. It requires higher values of capacitor and inductor as compared to the other PWM schemes. While using the THPWM, and SVPWM, the capacitor voltage ripple and inductor ripples are higher than that of MNSPWM. And it can be observed based on the mathematical analysis that optimal modulation index value is more for MNSPWM scheme than other PWM schemes. The designed capacitor and inductor values are also less for MNSPWM for a desired output voltages. Further, it is observed that the switching voltage stress using the MNSPWM schemes is less because of the biased reference waveform decreasing the charging time of the inductor.

Fig. 8a and 8b shows the plots of "ac gain vs dc gain" and "ac gain vs modulation" respectively. It is observed that, the MNSPWM gives more ac gain with a less modulation index than other schemes. So, using MNSPWM to NSBI requires a less input dc voltage, to produces a desired six phase output voltages.

III. SIMULATION AND HARDWARE RESULTS

The proposed NSBI along with six-phase machine is simulated using MATLAB/Simulink for $V_{dci} = 80V$. The inductors and the capacitor of the NSBI are selected based on (35) and (36), while considering the capacitor ripple voltage of 5%, and inductor ripple current of 5% switching frequency $f_s = 5kHz$. Also, a laboratory prototype of NSBI was developed using SEMIKRON SKM100GB12T4 power IGBTs and SPARTAN-6 FPGA controller as shown in Fig. 9 to control the 2 pole, six-phase induction motor. For experimental setup the inductor and capacitor values considered are the same as that of the simulation. The gating signals are generated using VHDL code

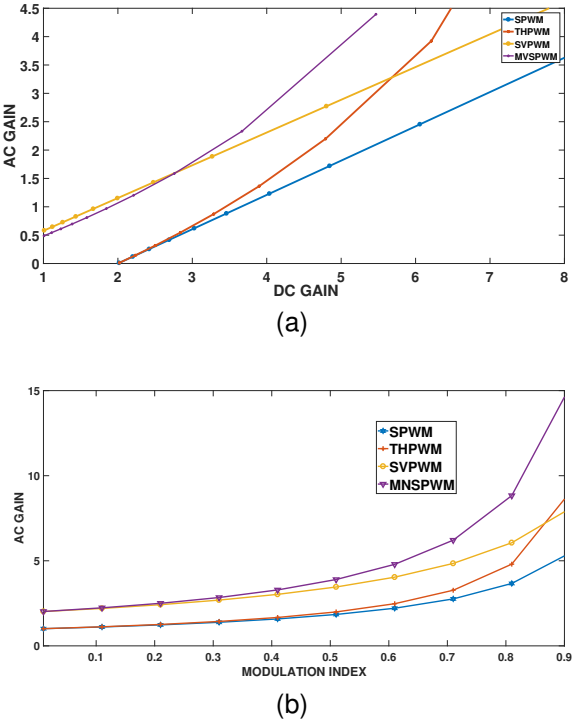

Fig. 8. Comparison of all PWMs a) ac gain vs dc gain, b) ac gain vs modulation index.

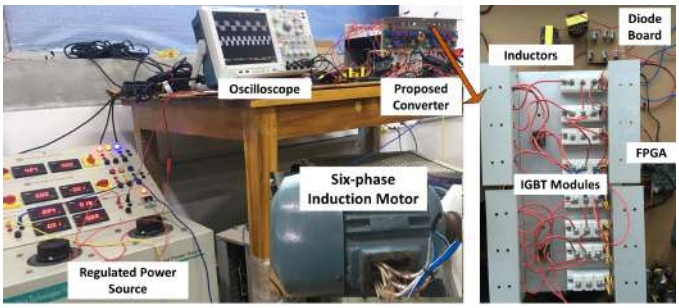

Fig. 9. Experimental setup of the NSBI fed to a six-phase motor is implemented using SPARTAN-6 XC6SLX9 FPGA control board, SKM100GB12T4 power IGBT modules, inductors, capacitors, and dc input source.

in FPGA control board and these gating signals are given to the respective switches through the gate driver circuit.

The performance of the NSBI is analyzed for various operational aspects as follows:

A. Normal Operation

The derived optimal value of modulation index $m_a = 0.677$ for symmetrical and $m_a = 0.794$ for asymmetrical winding are considered during the normal operation of the proposed six-phase drive. Fig. 10a shows the output voltage waveforms of upper and lower inverters of proposed NSBI for a given input voltage(V_{dci}) of 80 volts. These voltages are applied to the stator of six-phase machine. It is observed that, six stator voltages are separated by 60^0 and having an amplitude of 230V are used for the symmetrical operation. The speed and torque of six phase machine are given in Fig. 10b. The stator and rotor currents of six-phase machine are shown in Fig. 10c.

This article has been accepted for publication in a future issue of this journal, but has not been fully edited. Content may change prior to final publication. Citation information: DOI 10.1109/TTE.2020.3010337, IEEE Transactions on Transportation Electrification

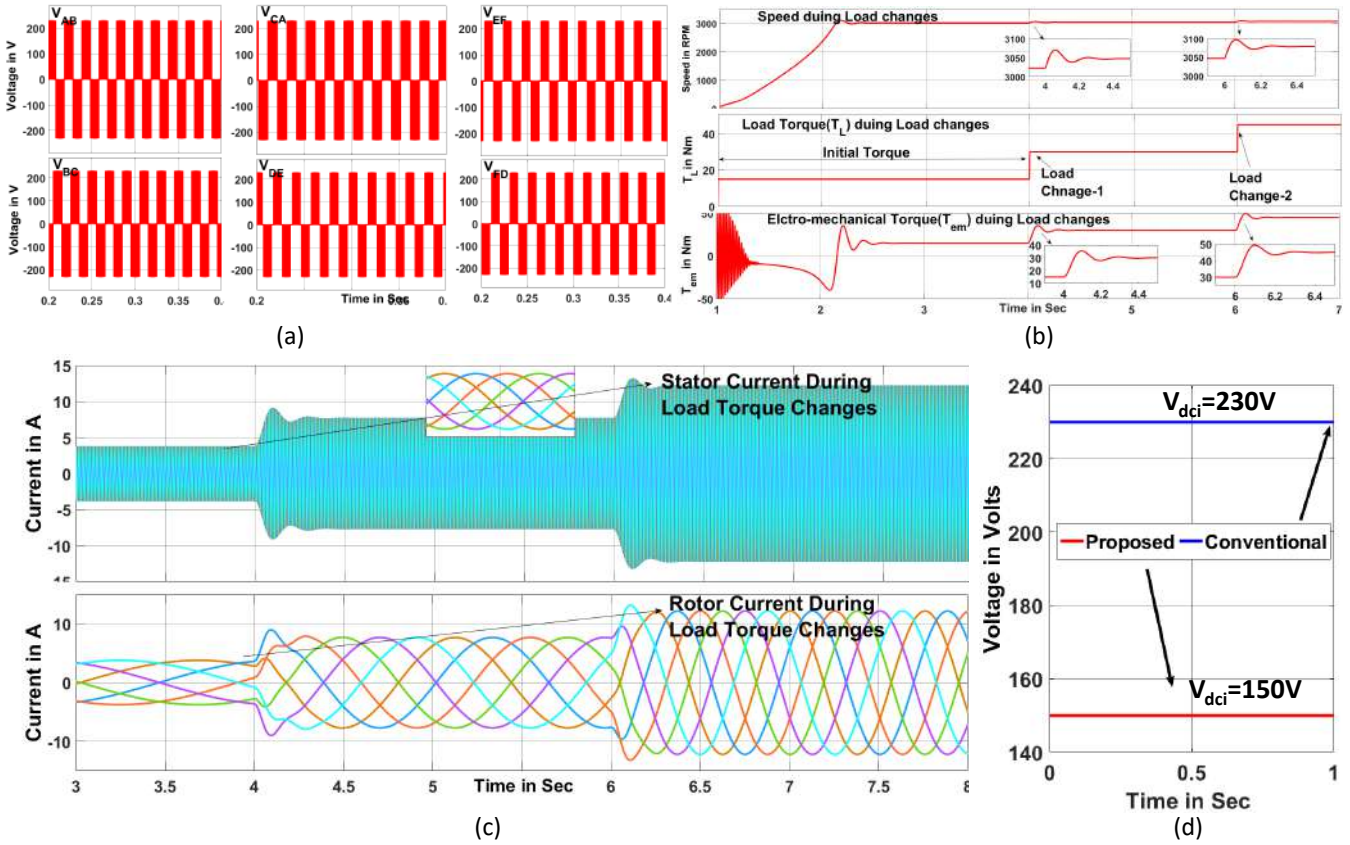

Fig. 10. Normal operation wave forms a) The voltage of upper and lower inverter of NSBI fed to six-phase induction motor, b) The torque and speed of the six-phase induction motor during normal operation and load changes, c) The stator currents of six-phase induction motor during normal operation and load torques changes, d) Dc-link voltage utilization of proposed and conventional converters.

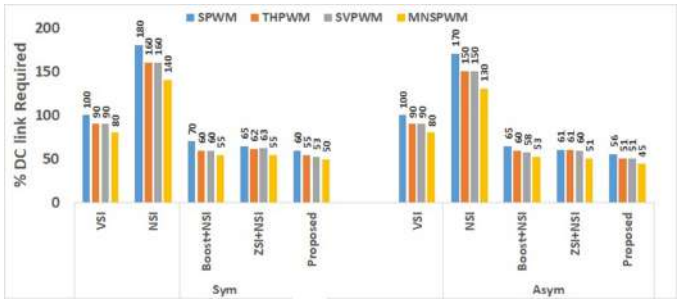

Fig. 11. % dc-link requirement of conventional and proposed converters.

It is observed that, initially the motor runs with an oscillated torque until it reaches to the rated speed of 3000rpm. Once the speed reaches to rated value, the torque remains constant. If the load torque T_L increases, then the speed decreased slightly and T_{em} increase smoothly. According to the load torque, the stator and rotor currents are increased. The smooth transition of speed, stator and rotor current, torque gives the better performance of six phase drive.

The dc-link voltage of conventional VSI and proposed converter are shown in Fig. 10d. The utilization of dc link is improved in proposed converter as compared to the conventional VSI. For the given speed and torque, the required input voltage for conventional VSI is 230V, where as this value is 150V for proposed converter. So by using the proposed converter, 21% dc-link is utilized more than the conventional VSI. Because of this, the proposed six-phase NSBI drive is suitable for low voltage battery powered electrical vehicles.

In general, the electrical vehicles are equipped with battery banks, which are connected in series to match the voltage requirement of the induction motor connected through the conventional VSI. An additional boost converter is required along with VSI to match the voltage requirement of the induction motor. So, when compared to the conventional VSI, the proposed NSBI requires less input dc voltage to drive the six phase induction motor. In this intent, the requirement of dc input voltage will reduce and less number of batteries will be sufficient. And also, the proposed NSBI provides six-phase voltage in a single stage conversion.

Fig. 11 shows the percentage dc input voltages required for producing the desired output voltage by various converter topologies using asymmetrical and symmetrical winding configurations. It is observed that, NSI requires double the input voltage than the VSI. But NSBI requires lesser input voltage than VSI.

Fig. 12 shows the hardware results of six-phase currents and voltages under normal operation. These hardware results resemble the simulation results. It is observed that, the six-phase currents of the drive are separated by 60^0 during symmetrical operation. The stator voltages and currents of

This article has been accepted for publication in a future issue of this journal, but has not been fully edited. Content may change prior to final publication. Citation information: DOI 10.1109/TTE.2020.3010337, IEEE Transactions on Transportation Electrification

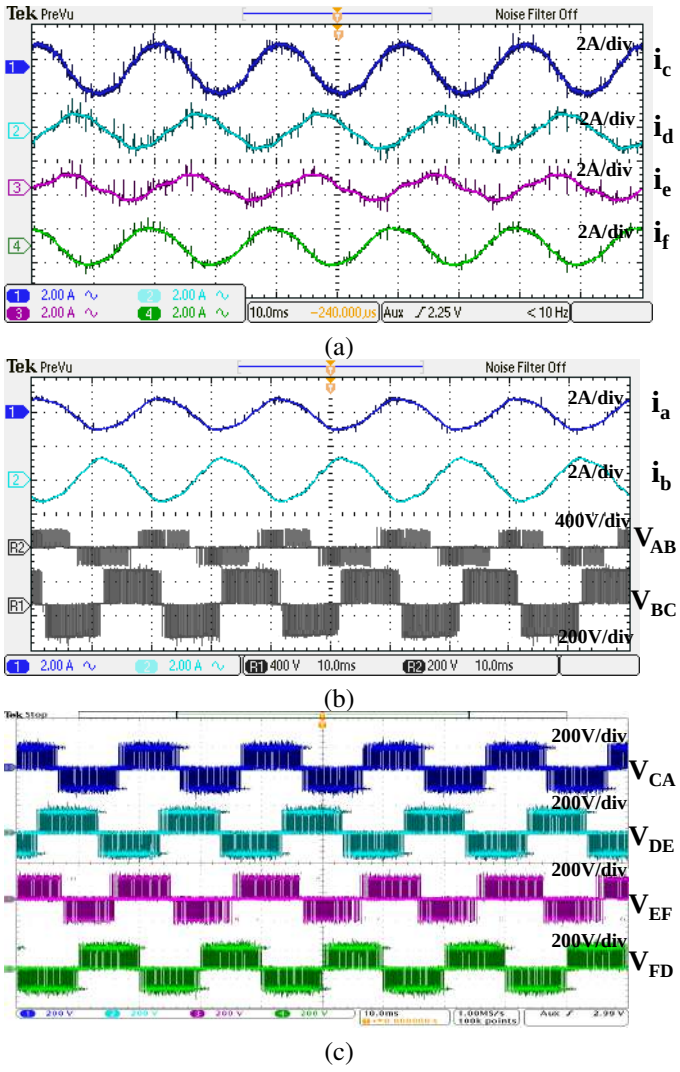

Fig. 12. The six phase currents and voltages of NSBI during normal operation.

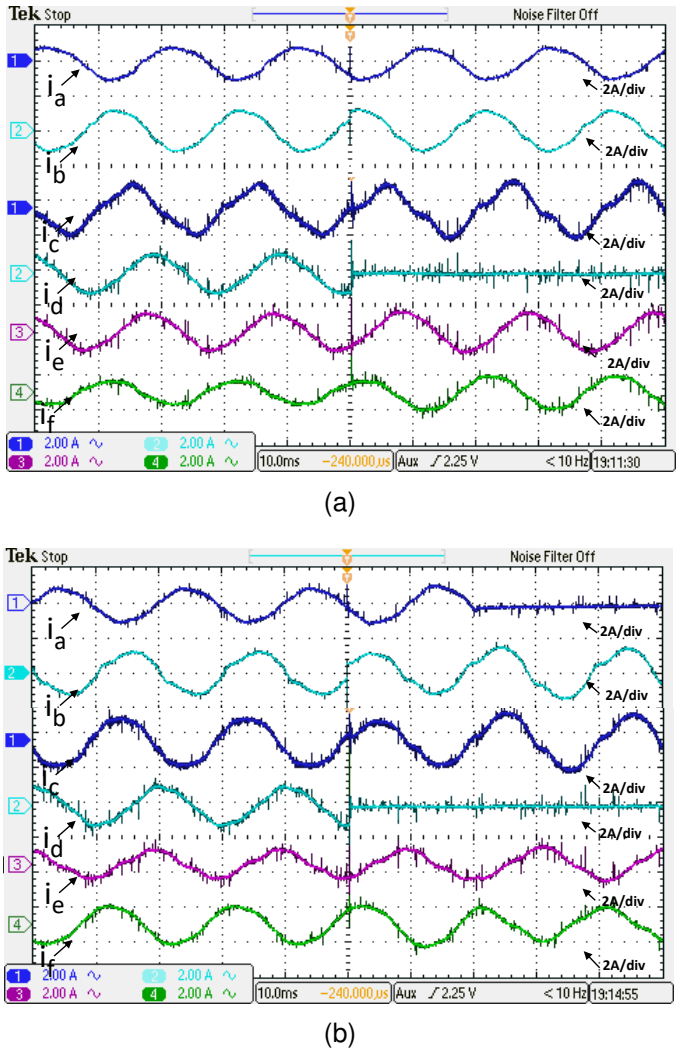

Fig. 13. The six phase currents of NSBI fed to six-phase induction motor during a) single faulty winding, b) dual faulty windings.

NSBI drive are observed as $230V$ and $1A$ for a given input voltage of $80V$. Also, it is able to provides variable frequency outputs for variable frequency drive applications [29].

B. Winding Failure

Single phase winding and dual phase winding failure conditions of six-phase induction motor is tested by opening the "$phase - d$" and "$phase - a$ & $phase - d$" of stator winding respectively under normal operating condition. The stator currents are plotted in Fig. 13a for single phase winding failure conditions. It is observed that, stator d-phase current becomes zero and the currents on other phases of same set (e-phase and f phase) are increased, but the currents on another set of three phases are not disturbed because of different neutrals of the upper and lower inverters. Similarly, the stator currents are plotted in Fig. 13b for dual phase winding failure conditions. From the result, it is observe that, the a-phase and d-phase currents become zero, because of two phases on different sets are open, then the currents of all other phases (b, c, e, f-phases) are increased. During the single winding open fault conditions, the motor continue to run as a 5-phase motor and dual winding fault conditions, the motor continue to run as a 4-phase motor with some vibrations and noise. Table IV gives the information of phase currents during single and dual phase winding failures.

TABLE IV
PHASE CURRENTS DURING WINDING FAILURE CONDITIONS

fault	$i_a(A)$	$i_b(A)$	$i_c(A)$	$i_d(A)$	$i_e(A)$	$i_f(A)$
Normal	1	1	1	1	1	1
d-phase	1	1	1	0	1.1	1.1
a and d phase	0	1.2	1.2	0	1.2	1.2

IV. CONCLUSION

This paper proposes a nine switch boost hybrid converter suitable for six-phase induction motor drive application. The proposed NSBI provides six -phase boost outputs in single stage conversion from a single input dc voltage source. And the proposed system improves the dc-link voltage utilization. When compared to other topologies (VSI, NSI, Boost+NSI, ZSI+NSI) the proposed NSBI requires lesser input dc voltage

to drive the six-phase induction motor. The main features of proposed NSBI drive are: it provides six phase boost ac outputs in single stage conversion; higher voltage gains; continuous dc-link voltage and input currents; it can operate during winding failure conditions as a reduced phase machine like 5-phase or 4-phase.

ACKNOWLEDGMENT

The authors would like to thank the Science and Engineering Research Board (SERB), a statutory body under the Department of Science and Technology, Government of India, for providing financial support to carry out this research work under the Project No: EMR/2016/003957.

REFERENCES

[1] E. Levi, R. Bojoi, F. Profumo, H. Toliyat, and S. Williamson, "Multi-phase induction motor drives–a technology status review," *IET Electric Power Applications*, vol. 1, no. 4, pp. 489–516, 2007.

[2] A. G. Yepes, J. A. Riveros, J. Doval-Gandoy, F. Barrero, O. López, B. Bogado, M. Jones, and E. Levi, "Parameter identification of multi-phase induction machines with distributed windings—part 1: Sinusoidal excitation methods," *IEEE Transactions on Energy Conversion*, vol. 27, no. 4, pp. 1056–1066, 2012.

[3] L. Parsa and H. A. Toliyat, "Fault-tolerant interior-permanent-magnet machines for hybrid electric vehicle applications," *IEEE Transactions on Vehicular Technology*, vol. 56, no. 4, pp. 1546–1552, 2007.

[4] A. Mohammadpour, S. Sadeghi, and L. Parsa, "A generalized fault-tolerant control strategy for five-phase pm motor drives considering star, pentagon, and pentacle connections of stator windings," *IEEE Transactions on Industrial Electronics*, vol. 61, no. 1, pp. 63–75, 2013.

[5] S. Rangari, H. Suryawanshi, and M. Renge, "New fault-tolerant control strategy of five-phase induction motor with four-phase and three-phase modes of operation," *Electronics*, vol. 7, no. 9, p. 159, 2018.

[6] O. Jasim, M. Sumner, C. Gerada, and J. Arellano-Padilla, "Development of a new fault-tolerant induction motor control strategy using an enhanced equivalent circuit model," *IET electric power applications*, vol. 5, no. 8, pp. 618–627, 2011.

[7] H. Guzman, M. J. Duran, F. Barrero, B. Bogado, and S. Toral, "Speed control of five-phase induction motors with integrated open-phase fault operation using model-based predictive current control techniques," *IEEE Transactions on Industrial Electronics*, vol. 61, no. 9, pp. 4474–4484, 2013.

[8] S. Dwari and L. Parsa, "Fault-tolerant control of five-phase permanent-magnet motors with trapezoidal back emf," *IEEE transactions on industrial electronics*, vol. 58, no. 2, pp. 476–485, 2010.

[9] A. S. Salem, R. A. Hamdy, A. S. Abdel-Khalik, I. F. El-Arabawy, and M. S. Hamad, "Performance of nine-switch inverter-fed asymmetrical six-phase induction machine under machine and converter faults," in *IEEE 2016 Eighteenth International Middle East Power Systems Conference (MEPCON)*, pp. 711–716, 2016.

[10] D. Glose and R. Kennel, "Carrier-based pulse width modulation for symmetrical six-phase drives," *IEEE Transactions on Power Electronics*, vol. 30, no. 12, pp. 6873–6882, 2015.

[11] N. Jarutus and Y. Kumsuwan, "Discontinuous and continuous space vector modulations for a nine-switch inverter," in *2016 IEEE 8th InternationalPower Electronics and Motion Control Conference (IPEMC-ECCE Asia)*, pp. 581–588, 2016.

[12] K. Kumar and K. Sivakumar, "A quad two-level inverter configuration for four-pole induction-motor drive with single dc link," *IEEE Transactions on Industrial Electronics*, vol. 62, no. 1, pp. 105–112, 2015.

[13] Y. P. Kumar and B. Ravikumar, "A simple modular multilevel inverter topology for the power quality improvement in renewable energy based green building microgrids," *Electric Power Systems Research*, vol. 140, pp. 147–161, 2016.

[14] K. K. Nallamekala and K. Sivakumar, "A fault-tolerant dual three-level inverter configuration for multipole induction motor drive with reduced torque ripple," *IEEE Transactions on Industrial Electronics*, vol. 63, no. 3, pp. 1450–1457, 2016.

[15] G. Singh and A. Iqbal, "Modeling and analysis of six-phase synchronous motor under fault condition," *Chinese Journal of Electrical Engineering*, vol. 3, no. 2, pp. 62–75, 2017.

[16] M. Forouzesh, Y. P. Siwakoti, S. A. Gorji, F. Blaabjerg, and B. Lehman, "Step-up dc–dc converters: A comprehensive review of voltage-boosting techniques, topologies, and applications," *IEEE Transactions on Power Electronics*, vol. 32, no. 12, pp. 9143–9178, 2017.

[17] V. Jagan, J. Kotturu, and S. Das, "Enhanced-boost quasi-z-source inverters with two-switched impedance networks," *IEEE Transactions on Industrial Electronics*, vol. 64, no. 9, pp. 6885–6897, 2017.

[18] P. M. Kishore and R. Bhimasingu, "A simplified converter with simultaneous multi-level ac and boost dc outputs for hybrid microgrid applications," in *2016 IEEE International Conference on Power Electronics, Drives and Energy Systems (PEDES)*, pp. 1–6, 2016.

[19] O. Ray, A. P. Josyula, S. Mishra, and A. Joshi, "Integrated dual-output converter," *IEEE Transactions on Industrial Electronics*, vol. 62, no. 1, pp. 371–382, 2015.

[20] O. Ray and S. Mishra, "Boost-derived hybrid converter with simultaneous dc and ac outputs," *IEEE transactions on Industry applications*, vol. 50, no. 2, pp. 1082–1093, 2014.

[21] M. Sahoo and S. Keerthipati, "A three-level lc-switching-based voltage boost npc inverter," *IEEE Transactions on Industrial Electronics*, vol. 64, no. 4, pp. 2876–2883, 2017.

[22] Y. P. Siwakoti, F. Z. Peng, F. Blaabjerg, P. C. Loh, and G. E. Town, "Impedance-source networks for electric power conversion part i: A topological review," *IEEE Transactions on Power Electronics*, vol. 30, no. 2, pp. 699–716, 2015.

[23] Y. P. Siwakoti, F. Z. Peng, F. Blaabjerg, P. C. Loh, G. E. Town, and S. Yang, "Impedance-source networks for electric power conversion part ii: review of control and modulation techniques," *IEEE Transactions on Power Electronics*, vol. 30, no. 4, pp. 1887–1906, 2015.

[24] P. M. Kishore and R. Bhimasingu, "A split source boost switched capacitor multilevel inverter for low power applications," in *2017 IEEE National Power Electronics Conference (NPEC)*, pp. 1–6, 2017.

[25] A. Abdelhakim, P. Mattavelli, V. Boscaino, and G. Lullo, "Decoupled control scheme of grid-connected split-source inverters," *IEEE Transactions on Industrial Electronics*, vol. 64, no. 8, pp. 6202–6211, 2017.

[26] A. Abdelhakim, P. Mattavelli, P. Davari, and F. Blaabjerg, "Performance evaluation of the single-phase split-source inverter using an alternative dc–ac configuration," *IEEE Transactions on Industrial Electronics*, vol. 65, no. 1, pp. 363–373, 2018.

[27] A. Abdelhakim, P. Mattavelli, and G. Spiazzi, "Three-phase split-source inverter (ssi): Analysis and modulation," *IEEE Transactions on Power Electronics*, vol. 31, no. 11, pp. 7451–7461, 2016.

[28] M. Azizi, A. Fatemi, M. Mohamadian, and A. Y. Varjani, "Integrated solution for microgrid power quality assurance," *IEEE Transactions on Energy Conversion*, vol. 27, no. 4, pp. 992–1001, 2012.

[29] P. M. Kishore and R. Bhimasingu, "Boost multi-port converter with simultaneous isolated dc, non-isolated dc and ac outputs," in *44th Annual Conference of the IEEE Industrial Electronics Society (IECON-2018)*, pp. 1061–1066, 2018.

[30] S. S. Lee and Y. E. Heng, "Improved single-phase split-source inverter with hybrid quasi-sinusoidal and constant pwm," *IEEE Transactions on Industrial Electronics*, vol. 64, no. 3, pp. 2024–2031, 2017.

[31] S. M. D. Dehnavi, M. Mohamadian, A. Yazdian, and F. Ashrafzadeh, "Space vectors modulation for nine-switch converters," *IEEE Transactions on Power Electronics*, vol. 25, no. 6, pp. 1488–1496, 2010.

[32] N. Jarutus and Y. Kumsuwan, "A carrier-based phase-shift space vector modulation strategy for a nine-switch inverter," *IEEE Transactions on Power Electronics*, vol. 32, no. 5, pp. 3425–3441, 2017.

[33] S. M. Dehghan, A. Amiri, M. Mohamadian, and M. A. Andersen, "Modular space-vector pulse-width modulation for nine-switch converters," *IET Power Electronics*, vol. 6, no. 3, pp. 457–467, 2013.

[34] L. Zhang, P. C. Loh, and F. Gao, "An integrated nine-switch power conditioner for power quality enhancement and voltage sag mitigation," *IEEE Transactions on Power Electronics*, vol. 27, no. 3, pp. 1177–1190, 2012.

[35] K. Aganah, S. Karugaba, and O. Ojo, "Space vector and carrier-based pwm modulation schemes for maximum utilization of voltage sources of a nine-switch converter," in *2012 IEEE Energy Conversion Congress and Exposition (ECCE)*, pp. 2521–2528, 2012.

[36] M. S. Diab, A. A. Elserougi, A. S. Abdel-Khalik, A. M. Massoud, and S. Ahmed, "A nine-switch-converter-based integrated motor drive and battery charger system for evs using symmetrical six-phase machines," *IEEE Transactions on Industrial Electronics*, vol. 63, no. 9, pp. 5326–5335, 2016.

[37] F. Gao, L. Zhang, D. Li, P. C. Loh, Y. Tang, and H. Gao, "Optimal pulsewidth modulation of nine-switch converter," *IEEE Transactions on Power Electronics*, vol. 25, no. 9, pp. 2331–2343, 2010.

[38] G. N. Goyal and M. V. Aware, "A comparative performance of six-phase nine switch inverter operation with spwm and svpwm," in *2012 IEEE International Conference on Power Electronics, Drives and Energy Systems (PEDES)*, pp. 1–6, 2012.

[39] C. A. Reusser, "Full-electric ship propulsion, based on a dual nine-switch inverter topology for dual three-phase induction motor drive," in *2016 IEEE Transportation Electrification Conference and Expo (ITEC)*, pp. 1–6, 2016.

[40] K. Ali, P. Das, and S. K. Panda, "A special application criterion of the nine-switch converter with reduced conduction loss," *IEEE Transactions on Industrial Electronics*, vol. 65, no. 4, pp. 2853–2862, 2018.

[41] M. Azizi, M. Mohamadian, and R. Beiranvand, "A new family of multi-input converters based on three switches leg," *IEEE Transactions on Industrial Electronics*, vol. 63, no. 11, pp. 6812–6822, 2016.

[42] S. M. Dehghan, M. Mohamadian, and A. Yazdian, "Hybrid electric vehicle based on bidirectional z-source nine-switch inverter," *IEEE Transactions on Vehicular Technology*, vol. 59, no. 6, pp. 2641–2653, 2010.

[43] S. M. Dehghan, M. Mohamadian, A. Yazdian, and F. Ashrafzadeh, "A dual-input–dual-output z-source inverter," *IEEE Transactions on power electronics*, vol. 25, no. 2, pp. 360–368, 2010.

[44] P. Mohana Kishore and R. Bhimasingu, "Dual-input and triple-output boost hybrid converter suitable for grid-connected renewable energy sources," *IET Power Electronics*, vol. 13, no. 4, pp. 808–820, 2020.

[45] N. B. Araya, "Modelling and control of six-phase induction motor drive," Master's thesis, NTNU, 2012.

[46] A. Abdelhakim, P. Mattavelli, and G. Spiazzi, "Three-phase three-level flying capacitors split-source inverters: Analysis and modulation," *IEEE Transactions on Industrial Electronics*, vol. 64, no. 6, pp. 4571–4580, 2017.

Pinjala Mohana Kishore received the B.Tech. degree in Electrical and Electronics Engineering from the Jawaharlal Nehru Technology University (JNTU), Kakinada, India, in 2010, and the M.Tech. degree in Electrical Drives from National Institute of Technology Bhopal, India, in 2013. He is currently working toward the Ph.D. degree from the Department of Electrical Engineering, Indian Institute of Technology Hyderabad, India. His research interests include Multilevel inverters, Pulse width modulation techniques, DC-DC power converters, Multi-phase drives, and Grid integration of renewable energy sources.

Ravikumar Bhimasingu received the B.Tech degree in Electrical & Electronics Engineering from Nagarjuna University (A.P) in 2002 and M.Sc (Engg.) degree in 2004 and Ph.D. degree in 2009 both from the Department of Electrical Engineering, Indian Institute of Science, Bangalore, India. During 2010–2013, he worked as a Senior Executive-Technology at Global R& D centre, Crompton Greaves Ltd., Mumbai, India. He joined the department of Electrical Engineering, IIT Hyderabad as an Assistant Professor in July 2013. Currently, he is working as an Associate Professor at Indian Institute of Technology, Hyderabad, India. His research interests include Computer aided Power System analysis, Distribution Automation, AI techniques applications to Power Systems, Power System protection & optimization, Grid integration of renewable energy sources, and Protection & Control of Micro Grids.